Supplementary Information

Nanocar Swarm Movement on Graphene Surface

Mehran Vaezi[1], Hossein Nejat Pishkenari[2], Mohammad Reza Ejtehadi[3]*

[1]Institute for Nanoscience and Nanotechnology (INST), Sharif University of Technology, Tehran, Iran
[2] Mechanical Engineering Department, Sharif University of Technology, Tehran, Iran
[3] Department of Physics, Sharif University of Technology, Tehran, Iran

*Corresponding Author, Email: nejat@sharif.edu

Table of Contents

Section S1. The parameters employed for the simulation of nanocars

The following parameters of the molecular mechanics force field[1-3] have been utilized to simulate the motion of nanocars on graphene surface.

The bond terms were considered to be harmonic style.

$$E_{bond} = K_b(r - r_0)^2 \quad \text{(S1)}$$

Table S1. The parameters of the bond term

Interacting atoms	$K_b(ev/\text{Å}^2)$	$r_0(\text{Å})$
C2 C2	48.6652	1.212
C2 CA	30.8837	1.313
CA CA	25.1593	1.392
CA H	14.35	1.101
CA NA	34.596	1.260

The angle terms were considered as harmonic style, as well.

$$E_{angle} = K_a(\theta - \theta_0)^2 \quad \text{(S2)}$$

Table S2. The parameters of the angle term

Interacting atoms	$K_a(ev/rad^2)$	$\theta_0(rad)$
C2 C2 CA	1.46619	π
C2 CA CA	1.34141	$2\pi/3$
CA CA CA	1.34141	$2\pi/3$
CA CA H	1.12304	$2\pi/3$
CA CA NA	1.34141	$2\pi/3$
CA NA CA	1.34141	0.638π

The following equation describes the dihedral style.

$$E_{dihedral} = \frac{1}{2}K_{d1}(1 + \cos\alpha) + \frac{1}{2}K_{d2}(1 - \cos 2\alpha) \quad \text{(S3)}$$

$$+\frac{1}{2}K_{d3}(1+\cos 3\alpha)+\frac{1}{2}K_{d4}(1-\cos 4\alpha)$$

Table S3. Parameters of dihedral term

Interacting atoms	$K_{d1}(ev)$	$K_{d2}(ev)$	$K_{d3}(ev)$	$K_{d4}(ev)$
CA C2 C2 CA	0	4.34E-05	0	0
C2 C2 CA CA	0	4.34E-05	0	0
C2 CA CA CA	0	0.650451	0	0
C2 CA CA H	0	0.650451	0	0
CA CA CA CA	-0.0403	0.208144	0	0
CA CA CA H	0	0.234379	0.046	0
CA CA CA NA	0.0433	0.650451	0	0
H CA CA H	0	0.390271	0	0
H CA CA NA	0	0.650451	0	0
NA CA CA NA	0	0.433634	0	0
CA CA NA CA	0	0.433634	0	0

The vdW interactions were described by 6-12 Lennard-Jones potential.

$$E_{LJ}=4\varepsilon[\left(\frac{\sigma}{r}\right)^{12}-\left(\frac{\sigma}{r}\right)^{6}], \qquad r<r_{cut-off} \tag{S4}$$

Table S4. The parameters of the LJ potential

Interacting atoms	$\varepsilon(eV)$	σ(Å)
H H	0.00203	2.672
H C2	0.00197	3.646
H CA	0.00197	3.646
H NA	0.00220	2.957
C2 C2	0.00191	3.460
C2 CA	0.00191	3.460
C2 NA	0.00213	3.349
CA CA	0.00191	3.460
CA NA	0.00213	3.349
NA NA	0.00238	3.242

Table S5. The LJ parameters employed for the simulation of C60.

Interacting atoms	ε (eV)	σ (Å)
C C	0.00241	3.410

Table S6. The geometry of the stable nanocar

Atom ID	Atom Type	x(Å)	y(Å)	z (Å)	Atom ID	Atom Type	x(Å)	y(Å)	z (Å)
1	C2	-29.19	40.27	20.32	153	NA	-32.59	36.51	20.23
2	CA	-27.06	26.65	18.79	154	CA	-31.40	35.90	20.30
3	CA	-27.30	25.68	17.72	155	CA	-31.32	34.50	20.33
4	CA	-28.73	25.61	17.52	156	NA	-32.45	33.77	20.29
5	CA	-28.55	27.73	20.62	157	CA	-28.98	36.03	20.43
6	CA	-27.47	27.16	21.54	158	CA	-28.91	34.63	20.46
7	CA	-26.31	26.67	21.10	159	CA	-30.08	33.87	20.42
8	CA	-26.09	26.40	19.68	160	CA	-30.01	32.47	20.45
9	CA	-26.55	24.58	17.62	161	CA	-28.76	31.84	20.53
10	CA	-25.48	24.33	18.58	162	CA	-27.59	32.60	20.57
11	CA	-25.27	25.20	19.57	163	CA	-27.66	34.00	20.54
12	CA	-29.31	24.43	17.23	164	CA	-27.80	36.79	20.48
13	CA	-28.49	23.22	17.11	165	CA	-27.88	38.19	20.44
14	CA	-29.78	27.04	21.21	166	CA	-29.12	38.82	20.36
15	CA	-31.13	24.88	18.74	167	H	-31.25	38.55	20.25
16	CA	-30.56	24.05	17.86	168	H	-42.80	31.26	19.76
17	CA	-28.06	26.61	22.76	169	H	-42.93	33.73	19.73
18	CA	-29.49	26.54	22.55	170	H	-38.51	31.48	19.99
19	CA	-24.97	24.72	20.91	171	H	-43.02	35.45	19.70
20	CA	-25.61	25.63	21.86	172	H	-43.14	37.93	19.67
21	CA	-31.74	24.36	19.96	173	H	-38.86	38.15	19.89
22	CA	-31.48	25.31	21.03	174	H	-34.76	32.54	20.19
23	CA	-29.25	22.11	17.67	175	H	-35.01	37.50	20.09
24	CA	-30.53	22.62	18.13	176	H	-30.91	31.88	20.41
25	CA	-26.15	25.14	22.98	177	H	-26.63	32.11	20.64
26	CA	-27.43	25.66	23.45	178	H	-26.76	34.58	20.58
27	CA	-31.23	24.87	22.27	179	H	-26.84	36.30	20.54
28	CA	-30.19	25.51	23.06	180	H	-26.97	38.78	20.47
29	CA	-31.08	22.13	19.25	181	C2	-41.14	40.85	19.74
30	CA	-31.72	23.04	20.20	182	CA	-44.01	48.73	20.38
31	CA	-27.17	21.23	18.57	183	CA	-44.16	47.67	21.38
32	CA	-28.62	21.15	18.37	184	CA	-43.25	47.81	22.23
33	CA	-25.16	22.46	20.09	185	CA	-41.78	49.24	19.10
34	CA	-24.92	23.41	21.16	186	CA	-42.27	48.91	17.77
35	CA	-28.18	24.54	24.01	187	CA	-43.48	48.33	17.66
36	CA	-29.50	24.47	23.82	188	CA	-44.24	48.13	18.89
37	CA	-25.92	21.34	20.64	189	CA	-44.72	46.47	21.18
38	CA	-26.88	20.75	19.92	190	CA	-45.11	46.07	19.83
39	CA	-29.22	20.62	19.59	191	CA	-44.96	46.87	18.77
40	CA	-30.40	21.09	20.01	192	CA	-42.57	46.83	22.84
41	CA	-31.43	22.56	21.56	193	CA	-43.10	45.49	22.61
42	CA	-31.20	23.44	22.54	194	CA	-40.56	49.45	19.12
43	CA	-30.61	21.36	21.43	195	CA	-40.25	47.69	22.17
44	CA	-28.14	20.37	20.55	196	CA	-41.04	46.78	22.74
45	CA	-30.72	26.43	20.48	197	CA	-41.22	48.70	16.98
46	CA	-30.50	26.16	19.06	198	CA	-40.07	48.91	17.86
47	CA	-29.36	26.53	18.46	199	CA	-44.60	46.23	17.39
48	CA	-28.32	27.45	19.10	200	CA	-43.67	47.13	16.70

Atom ID	Atom Type	x(Å)	y(Å)	z (Å)	Atom ID	Atom Type	x(Å)	y(Å)	z (Å)
49	CA	-27.17	23.30	17.30	201	CA	-39.06	47.26	21.44
50	CA	-26.48	22.26	18.06	202	CA	-38.89	48.12	20.28
51	CA	-25.43	22.90	18.85	203	CA	-41.98	44.56	22.55
52	CA	-30.13	23.19	23.50	204	CA	-40.72	45.36	22.64
53	CA	-29.63	21.12	22.31	205	CA	-42.52	46.89	16.03
54	CA	-29.38	22.08	23.40	206	CA	-41.27	47.63	16.18
55	CA	-27.36	23.33	23.89	207	CA	-38.45	47.61	19.12
56	CA	-26.10	23.71	23.26	208	CA	-39.06	48.02	17.86
57	CA	-27.93	22.16	23.59	209	CA	-39.64	44.97	21.97
58	CA	-25.51	22.88	22.39	210	CA	-38.77	45.96	21.35
59	CA	-26.13	21.60	22.06	211	CA	-43.14	43.29	20.90
60	CA	-28.34	20.61	21.85	212	CA	-42.02	43.51	21.72
61	CA	-27.29	21.25	22.64	213	CA	-44.37	44.11	18.49
62	H	-28.33	28.48	18.73	214	CA	-44.23	44.95	17.31
63	C2	-28.63	29.19	20.58	215	CA	-40.17	46.66	16.19
64	C2	-28.69	30.39	20.56	216	CA	-39.11	46.85	16.99
65	CA	-40.47	25.99	22.28	217	CA	-43.27	43.15	18.50
66	CA	-39.61	25.01	22.95	218	CA	-42.68	42.74	19.63
67	CA	-38.36	24.97	22.22	219	CA	-40.83	43.09	20.98
68	CA	-40.44	27.11	19.94	220	CA	-39.70	43.80	21.09
69	CA	-41.85	26.52	19.86	221	CA	-38.29	45.40	20.09
70	CA	-42.49	26.00	20.92	222	CA	-38.13	46.19	19.02
71	CA	-41.78	25.72	22.16	223	CA	-38.86	44.06	19.93
72	CA	-40.13	23.89	23.47	224	CA	-41.22	42.30	19.72
73	CA	-41.56	23.62	23.36	225	CA	-39.99	49.09	20.28
74	CA	-42.34	24.50	22.73	226	CA	-40.83	48.82	21.45
75	CA	-37.72	23.80	22.08	227	CA	-42.16	48.94	21.36
76	CA	-38.27	22.58	22.65	228	CA	-42.78	49.35	20.10
77	CA	-39.76	26.48	18.71	229	CA	-44.10	45.32	21.83
78	CA	-37.21	24.30	19.77	230	CA	-44.16	44.17	20.94
79	CA	-37.17	23.43	20.78	231	CA	-44.81	44.58	19.71
80	CA	-42.13	25.99	18.53	232	CA	-38.54	45.72	17.71
81	CA	-40.76	25.97	17.78	233	CA	-39.21	43.61	18.72
82	CA	-43.40	24.03	21.85	234	CA	-39.06	44.49	17.56
83	CA	-43.49	24.95	20.73	235	CA	-40.74	45.32	16.04
84	CA	-37.41	23.84	18.41	236	CA	-42.24	45.49	15.94
85	CA	-38.21	24.84	17.82	237	CA	-40.20	44.29	16.70
86	CA	-38.00	21.48	21.73	238	CA	-42.97	44.56	16.54
87	CA	-37.33	22.00	20.51	239	CA	-42.38	43.43	17.26
88	CA	-43.76	24.48	19.50	240	CA	-40.33	42.59	18.48
89	CA	-43.02	25.01	18.33	241	CA	-41.05	43.28	17.32
90	CA	-39.11	24.39	16.94	242	H	-39.98	41.58	18.27
91	CA	-40.48	24.96	16.93	243	C2	-29.26	41.47	20.29
92	CA	-37.63	21.49	19.31	244	CA	-32.12	49.36	20.86
93	CA	-37.60	22.55	18.08	245	CA	-32.26	48.31	21.86
94	CA	-40.17	20.57	22.28	246	CA	-31.36	48.46	22.71
95	CA	-38.94	20.53	21.62	247	CA	-29.89	49.86	19.56
96	CA	-42.71	21.75	22.34	248	CA	-30.39	49.51	18.24
97	CA	-43.58	22.71	21.66	249	CA	-31.60	48.93	18.14
98	CA	-42.77	23.90	17.42	250	CA	-32.36	48.75	19.37
99	CA	-41.41	23.88	16.66	251	CA	-32.83	47.11	21.68
100	CA	-42.44	20.66	21.41	252	CA	-33.23	46.69	20.34
101	CA	-41.24	20.07	21.39	253	CA	-33.08	47.48	19.27

Atom ID	Atom Type	x(Å)	y(Å)	z (Å)	Atom ID	Atom Type	x(Å)	y(Å)	z (Å)
102	CA	-39.16	20.00	20.27	254	CA	-30.68	47.49	23.33
103	CA	-38.64	20.48	19.01	255	CA	-31.20	46.15	23.12
104	CA	-38.41	22.11	17.39	256	CA	-28.67	50.07	19.58
105	CA	-39.22	22.95	16.72	257	CA	-28.35	48.34	22.64
106	CA	-38.95	20.87	17.94	258	CA	-29.15	47.44	23.23
107	CA	-40.60	19.78	20.43	259	CA	-29.34	49.29	17.45
108	CA	-38.55	25.91	18.75	260	CA	-28.19	49.51	18.32
109	CA	-37.92	25.57	19.93	261	CA	-32.72	46.83	17.89
110	CA	-38.45	25.91	21.11	262	CA	-31.80	47.72	17.20
111	CA	-39.68	26.81	21.26	263	CA	-27.16	47.90	21.91
112	CA	-39.42	22.62	23.32	264	CA	-27.01	48.75	20.74
113	CA	-40.42	21.57	23.12	265	CA	-30.08	45.21	23.06
114	CA	-41.74	22.19	23.16	266	CA	-28.83	46.02	23.14
115	CA	-40.63	22.63	16.55	267	CA	-30.64	47.47	16.52
116	CA	-40.26	20.60	17.82	268	CA	-29.39	48.21	16.65
117	CA	-41.12	21.49	17.06	269	CA	-26.57	48.23	19.59
118	CA	-43.32	22.68	18.04	270	CA	-27.18	48.62	18.33
119	CA	-43.93	23.04	19.32	271	CA	-27.75	45.61	22.47
120	CA	-42.66	21.52	17.92	272	CA	-26.88	46.60	21.83
121	CA	-43.82	22.22	20.37	273	CA	-31.25	43.93	21.44
122	CA	-43.15	20.93	20.17	274	CA	-30.13	44.15	22.25
123	CA	-41.04	20.04	18.92	275	CA	-32.49	44.72	19.02
124	CA	-42.60	20.64	18.98	276	CA	-32.36	45.54	17.82
125	H	-39.46	27.83	21.58	277	CA	-28.30	47.25	16.67
126	C2	-40.51	28.57	19.92	278	CA	-27.24	47.45	17.47
127	C2	-40.57	29.76	19.90	279	CA	-31.39	43.76	19.03
128	C2	-41.08	39.65	19.76	280	CA	-30.80	43.36	20.17
129	CA	-30.29	38.06	20.31	281	CA	-28.94	43.73	21.51
130	CA	-30.22	36.66	20.35	282	CA	-27.81	44.43	21.61
131	CA	-41.89	31.85	19.81	283	CA	-26.41	46.03	20.58
132	CA	-41.97	33.24	19.79	284	CA	-26.25	46.81	19.51
133	CA	-40.79	34.01	19.84	285	CA	-26.98	44.69	20.44
134	CA	-39.55	33.37	19.91	286	CA	-29.33	42.93	20.26
135	CA	-39.48	31.97	19.93	287	CA	-28.10	49.72	20.73
136	CA	-40.65	31.21	19.88	288	CA	-28.94	49.46	21.91
137	CA	-40.87	35.41	19.82	289	CA	-30.27	49.58	21.83
138	CA	-42.11	36.04	19.75	290	CA	-30.89	49.97	20.57
139	CA	-42.18	37.44	19.72	291	CA	-32.21	45.97	22.35
140	CA	-41.01	38.20	19.78	292	CA	-32.27	44.80	21.47
141	CA	-39.76	37.57	19.85	293	CA	-32.92	45.20	20.23
142	CA	-39.69	36.17	19.87	294	CA	-26.66	46.32	18.20
143	CA	-38.45	35.53	19.94	295	CA	-27.33	44.22	19.23
144	CA	-38.37	34.13	19.96	296	CA	-27.18	45.09	18.07
145	NA	-37.32	36.26	19.99	297	CA	-28.86	45.91	16.54
146	CA	-36.13	35.65	20.06	298	CA	-30.36	46.08	16.44
147	CA	-36.06	34.26	20.09	299	CA	-28.32	44.88	17.21
148	NA	-37.18	33.53	20.04	300	CA	-31.10	45.14	17.06
149	CA	-34.81	33.62	20.17	301	CA	-30.50	44.02	17.79
150	CA	-33.64	34.38	20.21	302	CA	-28.45	43.20	19.01
151	CA	-33.71	35.78	20.19	303	CA	-29.17	43.88	17.85
152	CA	-34.96	36.42	20.11	304	H	-28.10	42.18	18.81

Section S2. Directionality of the motion of NC_2 cluster

The previous investigations indicated the role of molecular structures in the direction of the surface motion. The molecular dynamics study on the surface motion of carbon nanotubes (CNT) reported the directed motion of this nanostructure[4]. Due to the cylindrical symmetry of the carbon nanotube, the nanotubes with enough length prefer to move perpendicular to their axis. On the other hand, spherical-like molecules such as fullerene[5] and p-carborane[6] showed diffusive motion on the surface with uniform distribution of horizontal velocity in various directions on the surface. Here, we aim to evaluate the effect of the attachment of two nanocars on the direction of their surface motion. For this purpose, we obtain the distribution of the horizontal velocity for NC_1 and NC_2 clusters in different directions on the surface.

To calculate the distribution of the horizontal velocity, the velocities of the clusters COM were calculated relative to the graphene substrate at each time step. The direction of the motion was determined by computing the angle between the relative velocity and positive direction of the X axis. Next, the total velocity of cluster was obtained for each angle such as θ_0, by adding the magnitude of the clusters velocities at time steps that the direction of the motion is in θ_0. Considering the range of 0 to 360 for θ_0 angle, one can calculate the distribution of horizontal velocity of the clusters in different directions on the surface. It should be mentioned that, we considered the symmetrical structure of the graphene substrate by averaging the distribution of the horizontal velocity over 120^o intervals. Figure S1 demonstrates the distribution of the horizontal velocity for NC_1 and NC_2 clusters at the temperatures of 100 and 200 K. The NC_2 cluster is in the orientation #1 and the cluster maintain this orientation at the examined temperatures.

As we observe in Figure S1, the NC_1 and NC_2 clusters approximately experience similar horizontal velocities in different directions on graphene surface. The total horizontal velocity is distributed almost uniformly in different angles. As a result, no preferred direction can be reported for the motion of NC_2 cluster and single nanocar on graphene surface. The total value of velocity is considerably decreases in each direction by increasing the nanocars number and by decreasing the temperature. According to Figure S1, the distribution of the velocity of the single nanocar at 100 K is similar to the distribution of the velocity of NC_2 cluster at 200 K. The mentioned similarity in the distribution of horizontal velocity is confirmed by equipartition theorem.

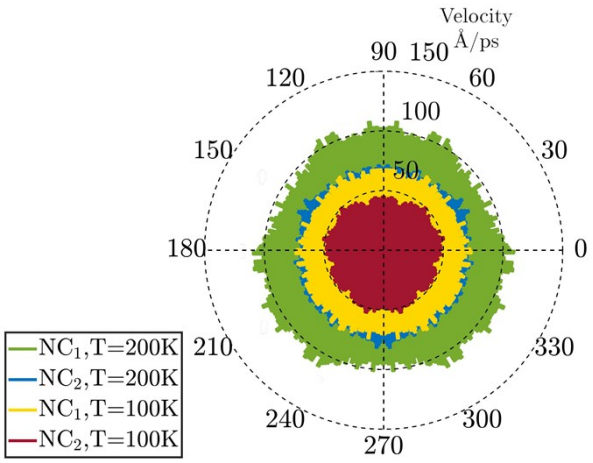

Figure S1. Distribution of the horizontal velocities of NC_1 and NC_2 clusters in different directions on the surface.

Section S3. Comparing the motion of fullerene clusters with nanocars

Figure S2a and S2b indicate the trajectories of the motion of nanocars and fullerenes clusters, respectively. In agreement with the previous results of the study, the mobility of the $C60_8$ cluster is considerably lower than the mobility of $C60_4$ at different temperatures. As we observe in Figure S2b, the $C60_8$ cluster experiences smaller displacements range compared with $C60_4$, which is attributed to the increase of vdW interactions between the molecules with the growth of fullerene number. According to the trajectories of the motion of fullerene clusters (Figure S2b), since the

clusters receive more thermal energy at higher temperatures, we observe the increase of displacements range with the temperature.

Comparing the trajectories of the motions of fullerenes with nanocars clusters reveals that, the displacements ranges of the mentioned clusters are on the same order. However, the clusters of nanocars experience smaller displacements compared with their corresponding fullerene clusters. The lower mobility of the nanocar clusters is likely related to the presence of chassis structure, which increases the strength of nonbonded interactions with the graphene substrate. Moreover, the fullerenes of nanocars are tightly bonded by the chassis, while the fullerene cluster has a flexible structure and the molecules change their positions in the cluster. As a result, the fullerenes of nanocar should simultaneously overcome the energy barriers against the surface motion; thus the nanocar experiences larger total energy barrier. On the other hand, since the molecules of fullerene cluster are less restricted, they are able to find paths with lower energy barrier during the motion on the graphene surface.

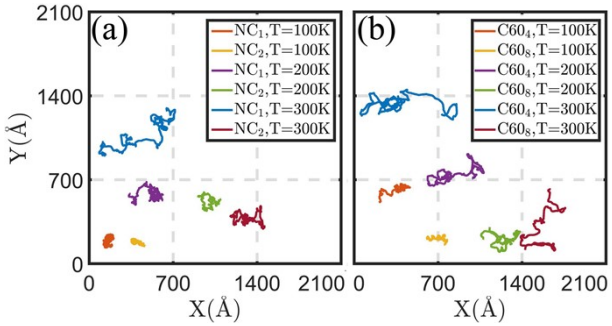

Figure S2. Trajectories of the motions of (a) nanocars and (b) fullerenes clusters at the temperatures of 100, 200 and 300 K. The clusters of nanocars including 1 and 2 nanomachines, while the fullerene clusters consist of 4 and 8 molecules.

The mean square displacements of the motions of clusters have been calculated. The variation of the MSDs confirms the change of the motion regime with respect to the population of the clusters. At each temperature, the fullerene/nanocar cluster with larger number of molecules experiences slower diffusion on graphene surface. Based on Figure S3a and S3b, the fullerene clusters indicate

higher values of MSDs in comparison with the nanocar clusters which have equal number of fullerenes. The structure of chassis increases the attraction energy between the nanocars and graphene surface, and consequently hinders the diffusion of nanocar clusters on the surface. Moreover, the lower MSDs of nanocars can be attributed to the higher energy barrier that nanocars experience on graphene surface.

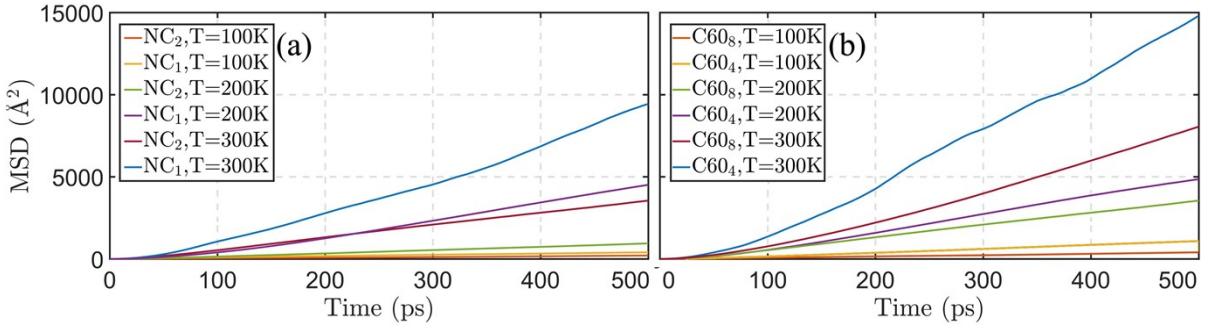

Figure S3. Mean square displacements of the motion of the clusters of (a) nanocars and (b) fullerenes.

Section S4. Surface motion of different orientations

In Figure S4, the trajectories of the motion of NC_2 center of mass are observable, while the nanocars are in orientations #1, #2 and #3. According to this figure, the nanocars with different orientations experience similar displacement range at the examined temperatures. As a result, the orientation of two nanocars does not affect the displacement range of the cluster on graphene surface.

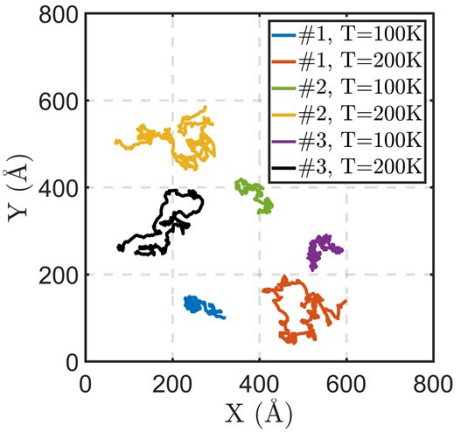

Figure S4. Trajectories of the surface motion of NC_2 cluster when the nanocars are in orientations #1, #2 and #3. The temperature of simulation system was adjusted to 100 and 200 K.

To evaluate the impact of nanocars orientation in the surface motion of cluster, the mean square displacement (MSD) has been calculated from the trajectories (Figure S4). Figure S5 illustrates the MSDs of the motion of NC_2 cluster, while the nanocars are positioned as orientations #1, #2 and #3. As we observe in this figure, the nanocars with different orientations indicate similar MSDs at the same temperatures. The MSD growth rate with respect to the temperature are also similar for the motion of NC_2 cluster at orientations #1 to #3, which implies that the surface motion of two nanocars with different orientations has similar diffusion coefficients on the graphene surface. Investigation on the surface motion of two nanocars constituting a cluster reveals that, the mobility of the cluster does not depend on the orientation of the nanocars.

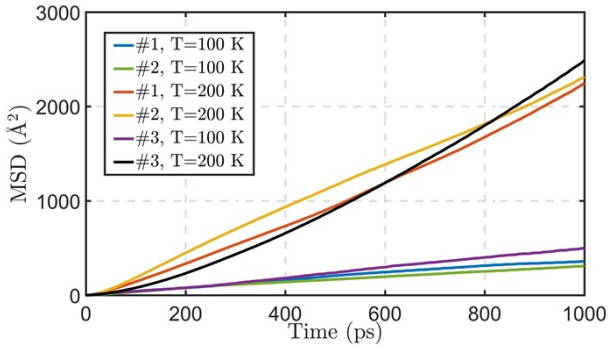

Figure S5. MSDs of the surface motion of NC_2 cluster at orientations #1, #2 and #3 and at the temperatures of 100 and 200 K.

Section S5. Mean square displacements of the clusters

Computing the mean square displacement of the clusters' COM, the surface diffusion of the groups was evaluated accurately. Figure S6 indicates the MSD of nanocar clusters obtained from the trajectories at temperature range of 100 to 400 K. Considering the number of nanocars, one can categorize the motion regime of clusters on graphene surface. While the single nanocar has significant MSD at different temperatures, nanocar clusters find notably lower MSD values which shows their restricted motion as a consequence of the growth of intermolecular attractions. In case

of larger nanocar clusters (e.g., NC5 and NC10), the groups indicate a low-mobility regime according to their MSD values. According to Figure S6, the increase of thermal energy at higher temperatures lets the nanocar clusters to diffuse further on the surface.

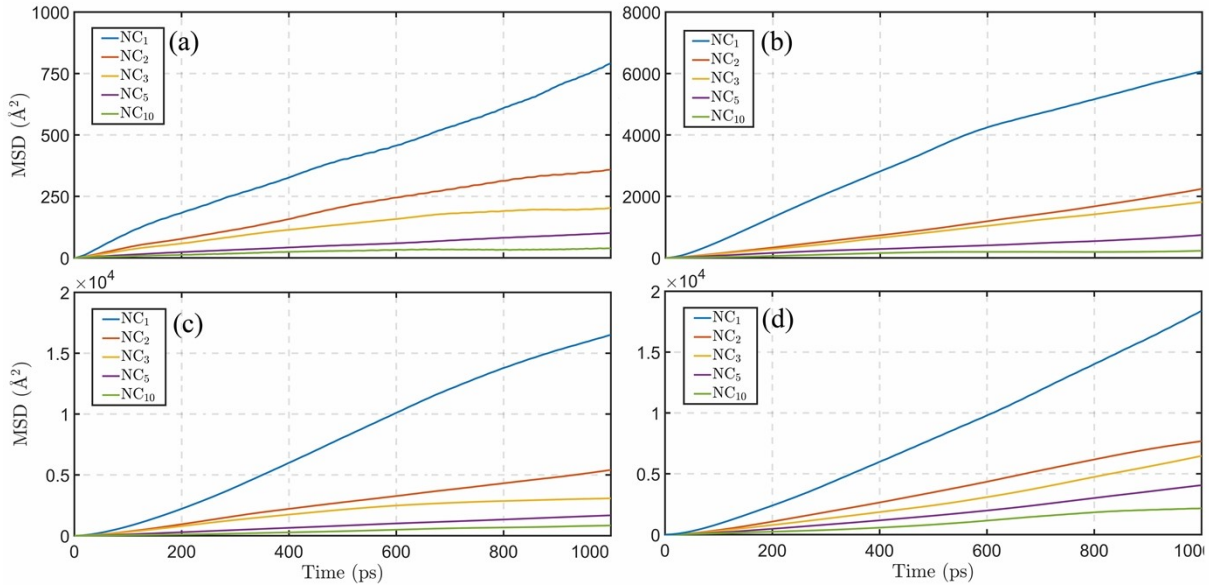

Figure S6. MSD of the motion of nanocar clusters as a function of time at the temperatures of (a) 100, (b) 200, (c) 300 and (d) 400 K.

Section S6. RMSD of the nanocars clusters

The configuration change of the NC_{10} cluster was characterized more precisely by calculating the root mean square deviation (RMSD). First, we removed the translational motions of the cluster center of mass at each time step. Next, the RMSD of the cluster was obtained using the following equation.

$$RMSD = \sqrt{\frac{1}{N}\sum_{j=1}^{N} |r'_f(j) - r'_i(j)|^2} \tag{S5}$$

where, N is the number of nanocars, r'_f and r'_i are the coordinates of the nanocars regardless of the translations at final and initial times, respectively. Since we consider the deviations for the

position of nanocars, an accurate investigation of the configuration change can be provided by this analysis. Figure S7 indicates the RMSD of the NC_{10} cluster at different temperatures. The RMSD has almost constant values at the temperatures of 100 and 200 K, which concludes the stable configuration of the cluster at these temperatures. As the temperatures rises to 300 K, we observe small variations in the RMSD of the cluster. Since the radius of gyration was constant at this temperatures, the small variation of RMSD can be attributed to the rotation of cluster. During the rotation of the cluster, the nanocars maintain their distance to the center of mass (R_g), while the position of nanocars changes in the cluster (RMSD).

By increasing the temperature to 400 and 500 K, the RMSD of the cluster saturates at higher values. The variation of RMSD at these temperatures reveals the change of configuration. At the temperature of 600 K, several considerable jumps are observed in the RMSD during the simulation time. The noticeable jumps of the RMSD demonstrates the separation of nanocars from the cluster. The RMSD finds values more than 100 Å at this temperature. The separation of nanocars can be inferred from the RMSD value at this temperature, because its value is close to the substrate dimensions.

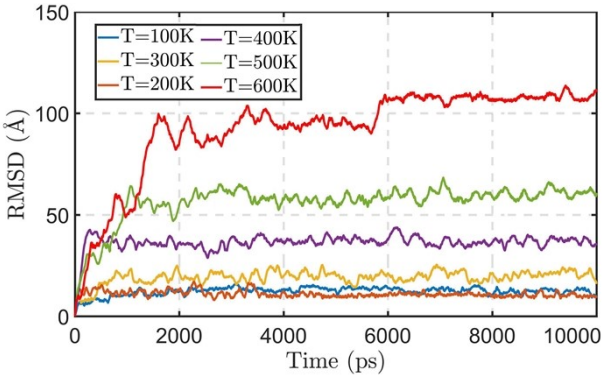

Figure S7. The RMSD of the NC_{10} cluster at the temperatures of 100, 200, 300, 400, 500 and 600 K.

Section S7. The chemical bonding of nanocar atoms at 600 K

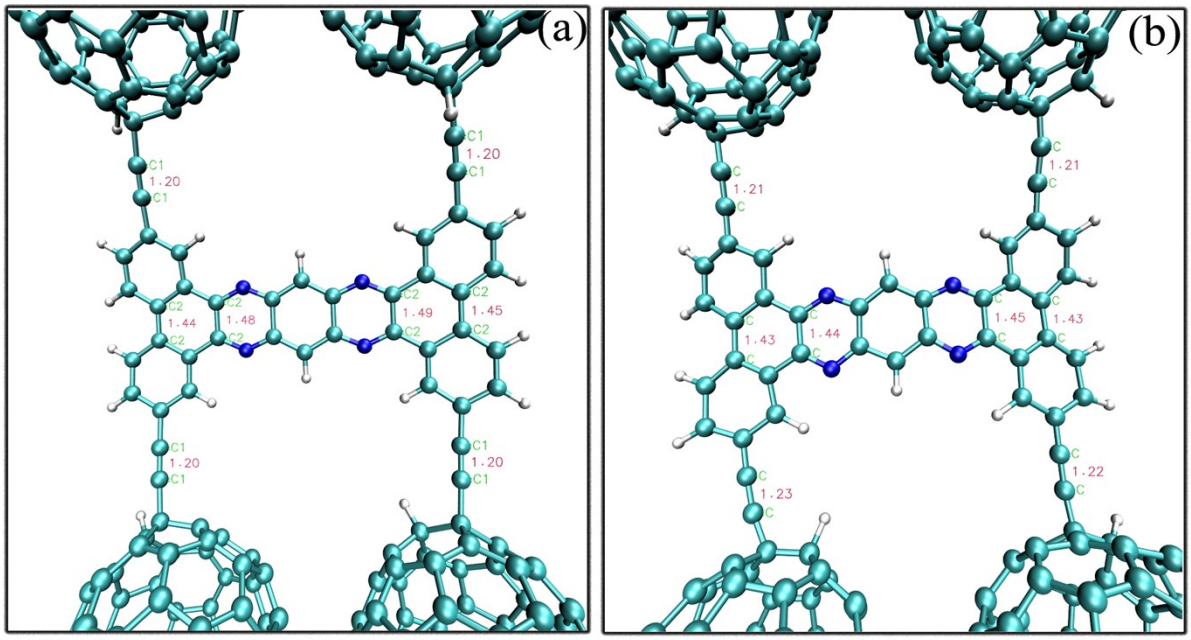

Figure S8. The chemical bonding of nanocar atoms obtained from the (a) ReaxFF and (b) molecular mechanics force-field, at the temperature of 600 K.

References:

1. Allinger, N. L.; Chen, K.; Lii, J. H., An Improved Force Field (Mm4) for Saturated Hydrocarbons. *Journal of computational chemistry* **1996**, *17*, 642-668.
2. Allinger, N. L.; Yuh, Y. H.; Lii, J. H., Molecular Mechanics. The Mm3 Force Field for Hydrocarbons. 1. *Journal of the American Chemical Society* **1989**, *111*, 8551-8566.
3. Allinger, N. L., Conformational Analysis. 130. Mm2. A Hydrocarbon Force Field Utilizing V1 and V2 Torsional Terms. *Journal of the American Chemical Society* **1977**, *99*, 8127-8134.
4. Kianezhad, M.; Youzi, M.; Vaezi, M.; Pishkenari, H. N., Rectilinear Motion of Carbon Nanotube on Gold Surface. *International Journal of Mechanical Sciences* **2021**, 107026.
5. Vaezi, M.; Nejat Pishkenari, H.; Nemati, A., Mechanism of C60 Rotation and Translation on Hexagonal Boron-Nitride Monolayer. *The Journal of Chemical Physics* **2020**, *153*, 234702.
6. Hosseini Lavasani, S. M.; Nejat Pishkenari, H.; Meghdari, A., Mechanism of 1, 12-Dicarba-Closo-Dodecaborane Mobility on Gold Substrate as a Nanocar Wheel. *The Journal of Physical Chemistry C* **2016**, *120*, 14048-14058.